Nonequivalence of Membrane Voltage and Ion-Gradient as Driving Forces for the Bacterial Flagellar Motor at Low Load

Chien-Jung Lo, Mark C. Leake, Teuta Pilizota, and Richard M. Berry
Clarendon Laboratory, Department of Physics, University of Oxford, Oxford, United Kingdom

ABSTRACT Many bacterial species swim using flagella. The flagellar motor couples ion flow across the cytoplasmic membrane to rotation. Ion flow is driven by both a membrane potential (V_m) and a transmembrane concentration gradient. To investigate their relation to bacterial flagellar motor function we developed a fluorescence technique to measure V_m in single cells, using the dye tetramethyl rhodamine methyl ester. We used a convolution model to determine the relationship between fluorescence intensity in images of cells and intracellular dye concentration, and calculated V_m using the ratio of intracellular/extracellular dye concentration. We found $V_m = -140 \pm 14$ mV in *Escherichia coli* at external pH 7.0 (pH_{ex}), decreasing to -85 ± 10 mV at pH_{ex} 5.0. We also estimated the sodium-motive force (SMF) by combining single-cell measurements of V_m and intracellular sodium concentration. We were able to vary the SMF between -187 ± 15 mV and -53 ± 15 mV by varying pH_{ex} in the range 7.0–5.0 and extracellular sodium concentration in the range 1–85 mM. Rotation rates for 0.35-μm- and 1-μm-diameter beads attached to Na^+-driven chimeric flagellar motors varied linearly with V_m. For the larger beads, the two components of the SMF were equivalent, whereas for smaller beads at a given SMF, the speed increased with sodium gradient and external sodium concentration.

INTRODUCTION

Many species of bacteria swim by rotating their flagella, using ion flux across the membrane to drive the flagellar motor (1,2). Ions are driven by the ion-motive force that comprises membrane potential (V_m) and ion gradient across the membrane (ΔpI). In *Escherichia coli* and *Vibrio alginolyticus*, motors are powered by proton (H^+) and sodium ion (Na^+) flux, respectively. Using tethered cells and polystyrene beads attached to flagella to measure the speed of rotation of the *E. coli* motor, it has been shown that the speed is proportional to protonmotive force (PMF) (3,4) and that under the high load imposed by tethered *Streptococcus* cells V_m and the proton gradient (ΔpH) are equivalent in driving the motor (5,6). However, in *E. coli*, V_m and ΔpH are strongly correlated and difficult to manipulate independently. As external pH decreases, internal pH also decreases, but not as much, so that the inward-directed ΔpH increases. At the same time, the inward-directed V_m decreases, but not enough to compensate for the increase of ΔpH, with the overall result that the PMF becomes larger (7). Variation of the speed of the *E. coli* motor in the pH range 4.7–8.8 (8) is consistent with the measured PMF variation and proportionality between speed and PMF.

In this work, we studied chimeric sodium-driven flagellar motors in *E. coli*, containing rotors from the proton-driven *E. coli* motor and stators that combine proteins from proton-driven *E. coli* and sodium-driven *V. alginolyticus* motors (9–11). To investigate the dependence of the motor mechanism on sodium-motive force (SMF), we developed a method to measure V_m in single cells using the Nernstian fluorescent dye, tetramethyl rhodamine methyl ester (TMRM). Combining this method with single-cell measurements of intracellular sodium concentration ($[Na^+]_{in}$) and motor speed (11), we demonstrated that V_m and ΔpNa in *E. coli* can be manipulated independently by external pH (pH_{ex}) and external sodium concentration ($[Na^+]_{ex}$), respectively. Using 1-μm-diameter beads to measure the rotation rate of the chimeric motor under high load, we found that speed is proportional to SMF, and that V_m and ΔpNa are equivalent in driving the motor. This confirms earlier, similar, results for the proton-driven motor. However, under low load with 0.35-μm-diameter beads, the speed was greater with high $[Na^+]_{ex}$ and a larger ΔpNa component of the SMF than with lower $[Na^+]_{ex}$ and a larger V_m component of the SMF. Thus, V_m and ΔpNa are not equivalent as driving forces for the flagellar motor, possibly indicating that the arrival of sodium ions is the rate-limiting step in low sodium concentration.

Quantitative measurement of V_m using cationic indicator dyes is based on equilibration of the dye across the membrane according to Boltzmann's law:

$$C_{in}/C_{ex} = exp(-qV_m/kT), \quad (1)$$

where k is Boltzmann's constant, T absolute temperature, q the charge of the dye, and C_{in} and C_{ex} the intracellular and extracellular dye concentrations, respectively. For a univalent cation, Eq. 1 can be rearranged to give the Nernst equation

$$V_m = -2.3\frac{kT}{e}\log\frac{C_{in}}{C_{ex}}. \quad (2)$$

Submitted August 14, 2006, and accepted for publication February 7, 2007.

Address reprint requests to Richard Berry, Clarendon Laboratory, Dept. of Physics, University of Oxford, Parks Rd., Oxford OX1 3PU, U.K. Tel.: 44-0-1865-282559; Fax: 44-0-1865-272400; E-mail: r.berry1@physics.ox.ac.uk.

Editor: Petra Schwille.

0006-3495/07/07/294/09 $2.00

doi: 10.1529/biophysj.106.095265

The dye should have high membrane permeability to ensure rapid equilibration and low toxicity to avoid perturbing the cell. C_{in} and C_{ex} are the concentrations of free dye in aqueous solution, as distinct from any dye molecules that are bound to the cell membrane or otherwise immobilized. Thus minimal binding of the dye to membranes and other intra- or extracellular components is desirable, so that the ratio C_{in}/C_{ex} can be determined accurately from fluorescence intensities. A typical bacterial membrane potential is around -150 mV, corresponding to $C_{in}/C_{ex} \approx 350$. This can lead to high concentrations of dye inside the cell, which can in turn lead to aggregation and quenching of fluorescence. Whereas this effect can be used as a qualitative indicator of V_m (12), quantitative measurements should avoid aggregation by using low concentrations of dye. Thus bright fluorescence, low photobleaching, and low aggregation and self-quenching are further desirable properties of the dye. Many hydrophobic membrane potential dyes have been designed to determine V_m of cells and mitochondria in vivo (13–16). In particular, the dye TMRM has been shown to be suitable for quantitative measurements of V_m in mitochondria (14).

Because bacteria (and mitochondria) are similar in size to the diffraction limit of a light microscope, the fluorescence intensity of pixels within the image of a single bacterium is not simply proportional to C_{in}, but also includes contributions from adjacent extracellular regions. Typically, C_{in} is greater than C_{ex}, thus the brightness of the cell image is reduced compared to a solution of the same concentration, and the ratio of internal to external fluorescence intensities underestimates the ratio C_{in}/C_{ex}. Loew's group has reported the measurement of V_m in individual mitochondria using TMRM fluorescence, correcting for the brightness reduction by measuring the point spread function (PSF) of the microscope and modeling the convolution process that reduces the brightness of the mitochondrial image (14,16). In this work, we adapted this technique to develop a single-cell fluorescence measurement of V_m in bacteria. We imaged *E. coli* cells immobilized at low density on a microscope coverslip, giving a very well-defined geometry well suited to optical convolution modeling. By using a high quantum-efficiency electron-multiplying charge-coupled device (EMCCD) camera, we obtained low-noise images using external TMRM concentrations of 0.1 μM and image exposure times of 10–30 ms. *E. coli* is a gram-negative bacterium with an outer membrane that acts as a barrier to the permeation of hydrophobic molecules such as TMRM. To increase the permeability of the dye with minimal damage to cell function, we pretreated cells with EDTA (11).

MATERIALS AND METHODS

Bacteria and cultures

E. coli strain YS34 (Δ*cheY, fliC*::*Tn10*, Δ*pilA*, Δ*motAmotB*) (10,11,17), with plasmid pYS11(*fliC* sticky filaments) and a second plasmid for inducible expression of stator proteins were used in our experiments. As described (11), chimeric stator proteins were expressed from plasmid pYS13 (*pomApotB7*^{E}), induced by isopropyl-β-D-thiogalactopyranoside and wild-type stator proteins were expressed from plasmid pDFB27 (*motAmotB*), induced by arabinose. Cells were grown in T-broth (1% tryptone (Difco, Detroit, MI), 0.5 % NaCl) for 5 h at 30°C from frozen stock containing the appropriate antibiotics and inducers (isopropyl-β-D-thiogalactopyranoside, 20 μM, or arabinose, 5 mM).

Sample preparation

Cells were suspended in sodium motility buffer (10 mM potassium phosphate, 85 mM NaCl, pH 7.0) plus 10 mM EDTA for 10 min to increase permeability to dye (11), then washed three times in sodium motility buffer. Cells at a density of 10^8 cells/ml were suspended in sodium motility buffer plus 0.1 μM TMRM (MIP, Ann Arbor, MI) and loaded into custom-built flow chambers (volume $\sim$5 μl), in which they were immobilized on polylysine-coated coverslips (11). For speed measurements, cells were sheared to truncate flagella, polystyrene beads (1.0 and 0.35 μm in diameter; Polysciences, Warrington, PA) were attached to flagella, and the speed/independent stator unit was measured using back-focal-plane interferometry or high-speed microscopy, as described (10,11,17,18). For each cell, speeds were calculated from the Fourier transform of bead position in data windows 1–5 s long beginning at 0.1-s intervals, for a total of 10–20 s. With low-level induction of stator proteins, speed histograms combining data from many cells under the same conditions showed distinct peaks corresponding to discrete numbers of stator units (see Fig. 4, *A* and *D*, and Reid et al. (17)). For 0.35-μm beads the speed with a single unit was obtained by a Gaussian fit to the slowest peak. For 1-μm beads the speed/unit was obtained by dividing the speeds with 1–5 units (obtained from a multiple-Gaussian fit to the speed histogram) by the number of units, and then averaging these five independent estimates. Intracellular sodium measurements were performed on single cells using the fluorescent indicator dye Sodium Green as described (11).

Microscopy

Cells were observed in epifluorescence using a custom-built microscope as described (11,19), except that TMRM was excited in epifluorescence mode at 532 nm by a diode-pumped solid-state laser (LCMT111-20, Laser2000, Northants, UK) via a dichroic mirror (530-nm long-pass). The total illuminated area was (20 μm)^2 and the illumination intensity at the sample was $\sim$5 W/cm^2 ($\pm$2%). The sample flow chamber was mounted on a piezoelectric stage (P-517.3cl, PI, Karlsruhe, Germany). Fluorescence emission was passed through the dichroic mirror, an emission filter (580-nm bandpass) and a notch rejection filter (532 nm) and imaged at 50 nm/pixel onto a cooled 128 $\times$ 128-pixel array of a back-illuminated EMCCD camera (iXon, DV860-BI, Andor, Belfast, UK). All experiments were performed at 23°C.

Internal fluorescence intensity

Images of bacteria with pixel intensities $I(x_i, y_i)$ were obtained with the focal plane passing through the center of the bacteria and an exposure time of 10–30 ms. The total fluorescence intensity (F_T) of a cell was defined as the average intensity of the central part of the cell, ignoring the marginal area and subtracting the background:

$$F_T = \langle I - I_{bg} \rangle_{I>I_0}, \quad (3)$$

where the background (I_{bg}) and threshold (I_o) intensities are as defined elsewhere (11). F_T includes fluorescence due to dye bound to the membrane (F_m) as well as fluorescence due to free dye (F_{in}). To estimate F_m, we treated cells, previously loaded for 30 min with TMRM and $[Na^+]_{ex} = 85$ mM, with 50 μM carbonyl cyanide 3-chlorophenylhydrazone (CCCP) for a further

30 min (see Fig. 2 *A*). CCCP collapses the membrane potential, under which condition we expect $V_m = 0$ and $C_{in} = C_{ex}$. Any remaining increased fluorescence of the cell compared to the background can be attributed to bound dye. We found that V_m (and therefore also C_{in} and F_m) depended strongly on pH_{ex} but only weakly on $[Na^+]_{ex}$, and we estimated, for each value of pH_{ex} studied,

$$F_m = \langle F_T \rangle_{cccp}, \tag{4}$$

where the average was taken over ~60 cells after loading and CCCP treatment as described above in buffers of the appropriate pH. The internal fluorescence due to free dye was estimated for each single-cell measurement as

$$F_{in} = F_T - F_m. \tag{5}$$

External fluorescence intensity

Due to the logarithmic nature of the Nernst equation, C_{in} will be ~350 times greater than C_{ex} when the $V_m = -150$ mV. If the camera exposure time were set to match the pixel intensities within the cell image to the full 14-bit dynamic range of the EMCCD, the external fluorescence intensity (F_{ex}) would be close to the noise level. Therefore, we obtained F_{ex} as follows. We filled the flow cell with 0.1 μM TMRM in sodium buffer and imaged empty areas with the focal plane 0.45 μm above the coverslip surface, corresponding to the height of the center of a cell. (The coverslip surface was easily found by searching for slight scratches.) We defined

$$F^*_{ex} = \langle I \rangle, \tag{6}$$

where the average was taken over the entire image. F^*_{ex} was measured at a given illumination laser power with different exposure times in the range 0.1–1.0 s, and F_{ex} was defined as the slope of a line fit of F^*_{ex} versus exposure time, multiplied by the exposure time for cell images, 10–30 ms.

Point spread function

The PSF, $P(x_i, y_i, z_i)$, was defined as the pixel intensity $I(x_i, y_i)$ in images of single 20-nm fluorescent beads (Molecular Probes, Eugene, OR) stuck to the coverslip at $x = y = 0$ and at a distance $-z_i$ below the focal plane. The piezoelectric stage was used to scan z_i over the range ± 2.5 μm in 50-nm intervals (the image pixels are 50 nm^2, giving a cubic grid). Three images with exposure times of 0.1 s were averaged for each z_i. The PSF was normalized after background subtraction and correcting for photobleaching (Fig. 1 *B*).

Optical convolution model

We created a 3D model of a chamber with an *E. coli* cell stuck to the surface (Fig. 1 *A*). The dye concentrations in the model are

$$C_i(x_i, y_i, z_i) = \begin{cases} 0 : z \le 0, \text{ glass} \\ C_{ex} : \text{ medium} \\ C_{in} : \text{ cell} \end{cases}, \tag{7}$$

where the subscript i indicates (50 nm)^3 voxels filling the model chamber. The cell is a cylinder (2 μm long, 0.9-μm diameter) capped by two hemispheres (0.9-μm diameter) and stuck to the surface. The remaining volume of the chamber, whose x, y, and z dimensions are 14 μm, 12 μm, and 3 μm, respectively, is filled with medium. The blurred image, with the focal plane set at a distance $z_0 = 0.45$ μm from the coverslip, equivalent to midcell height as used for experimental measurements, was calculated as the convolution of the dye distribution and the PSF:

$$I_m(x_j, y_j, z_0) = \Sigma_i [C_i(x_i, y_i, z_i) P(x_j - x_i, y_j - y_i, z_0 - z_i)], \tag{8}$$

where $I_m(x_j, y_j, z_0)$ was the modeled intensity of image pixel j (Fig. 1 *C*, *lower*). The internal fluorescence intensity F_{in} was calculated from the image I_m as described above for experimental data using Eqs. 3–5, with $F_m = 0$, and the external fluorescence intensity F_{ex} was calculated as the average pixel intensity in a simulated image with $C_{in} = C_{ex} = 0.1$ μM. We defined a correction factor $S(F_{in}/F_{ex}) = (C_{in}/C_{ex})/(F_{in}/F_{ex})$, where C_{in} and C_{ex} are the concentrations input to the model and F_{in} and F_{ex} are the calculated fluorescence intensities (Fig. 1 *D*, *inset*).

Calculation of V_m

We calculated V_m using the Nernst equation, Eq. 2, and the corrected concentration ratio

$$C_{in}/C_{ex} = (F_{in}/F_{ex})\, S(F_{in}/F_{ex}), \tag{9}$$

where F_{in} and F_{ex} were measured experimentally and the correction factor $S(F_{in}/F_{ex})$ was calculated using the optical convolution model.

RESULTS

Dye loading and response time

The bacterial outer membrane is a barrier to hydrophobic molecules such as the membrane potential dye TMRM. We increased the membrane permeability by pretreating cells with EDTA (11). The external TMRM concentration

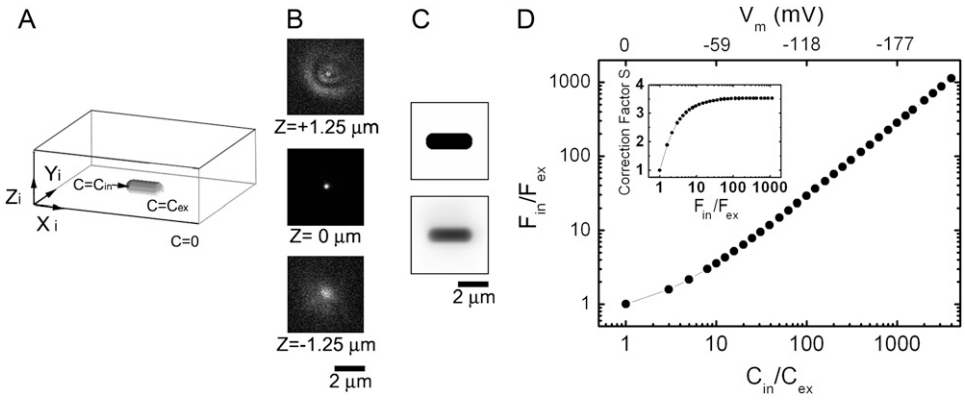

FIGURE 1 Calculation of the correction factor for convolution of the dye distribution with the microscope PSF. (*A*) Model of the dye distribution for a bacterium attached to a glass coverslip. (*B*) Cross sections of the measured PSF at different values of z. (*C*) Dye distribution at midcell height (*upper*) and the corresponding image after convolution (*lower*). (*D*) The calculated fluorescence intensity ratio, F_{in}/F_{ex}, versus the concentration ratio, C_{in}/C_{ex}. The correction factor, $S(F_{in}/F_{ex}) = (C_{in}/C_{ex})/(F_{in}/F_{ex})$, is also shown (*inset*). Fluorescence intensities were calculated from the convoluted image as described in the text.

$C_{ex} = 0.1$ μM was chosen to balance low membrane binding against sufficient fluorescence. After dye loading, we measured flagellar rotation to confirm that the motor and SMF were not affected by the dye. The mean and standard deviation of measured speed of 1-μm beads attached to the motor were determined from 26 nonloaded cells and 30 loaded cells in 85 mM $[Na^+]_{ex}$, pH 7. For nonloaded cells, the mean speed was 89 $\pm$ 6 Hz and the mean value of the standard deviations in speed for each cell was 1.8 $\pm$ 0.6 Hz; the corresponding values for loaded cells were 88 $\pm$ 6 Hz and 1.7 $\pm$ 0.8 Hz, indicating no significant effect of dye loading.

Fig. 2 *A* shows the total fluorescence intensity F_T during the loading of dye into live cells in different pH_{ex} (*solid symbols*). The fluorescence intensities increased exponentially to a steady state within ~30 min; exponential fits gave time constants of 10 $\pm$ 0.8, 14 $\pm$ 2, and 10 $\pm$ 2 min (mean $\pm$ SD) for pH 8, pH 7, and pH 6, respectively. The effect of 50 μM CCCP, a proton ionophore that eliminates the membrane potential, is shown for cells in pH 7 (*open circles*). F_T decreases exponentially (within ~30 min, fitted time constant 12 $\pm$ 3 min) to a stable nonzero value, $F_T = F_M$, indicating membrane binding of the dye (*dashed line*).

CCCP effect

The effect on cell fluorescence of 40 min incubation with a wide range of CCCP concentrations (0.1–50.0 μM), at pH 7, is shown in Fig. 2 *B* (*upper*). As in Fig. 2 *A*, the residual fluorescence intensity at high CCCP concentration is due to membrane binding of the dye. We estimated the fluorescence intensity due to membrane binding, F_m, as the average fluorescence intensity of cells treated with 50 μM CCCP (Methods). Fig. 2 *B* (*lower*) shows the membrane voltage, V_m, calculated as described in Methods, as a function of CCCP concentration. V_m decreases to zero with increasing [CCCP], indicating that CCCP may be used to achieve low values of V_m in experiments to investigate motor speed or other physiological functions. However, there was considerable intercellular variation in the value of V_m at a given CCCP concentration, as indicated by the large standard deviation (Fig. 2 *B, lower*, *error bars*). This illustrates the need to measure V_m in each cell if CCCP is to be used to control V_m.

Dependence of V_m and ΔpNa upon pH_{ex} and $[Na^+]_{ex}$

Fig. 3 *A* shows the dependence of V_m on pH_{ex} for *E. coli* cells expressing either sodium-driven chimeric or proton-driven wild-type flagellar motors. V_m decreases from -140 ± 14 to -85 ± 10 mV as pH changes from 7 to 5 with chimeric motors, and from -134 ± 17 to -85 ± 13 mV with wild-type motors. We previously showed that sodium influx through the chimeric motors is a significant part of the total sodium flux in a cell (11). The absence of any significant

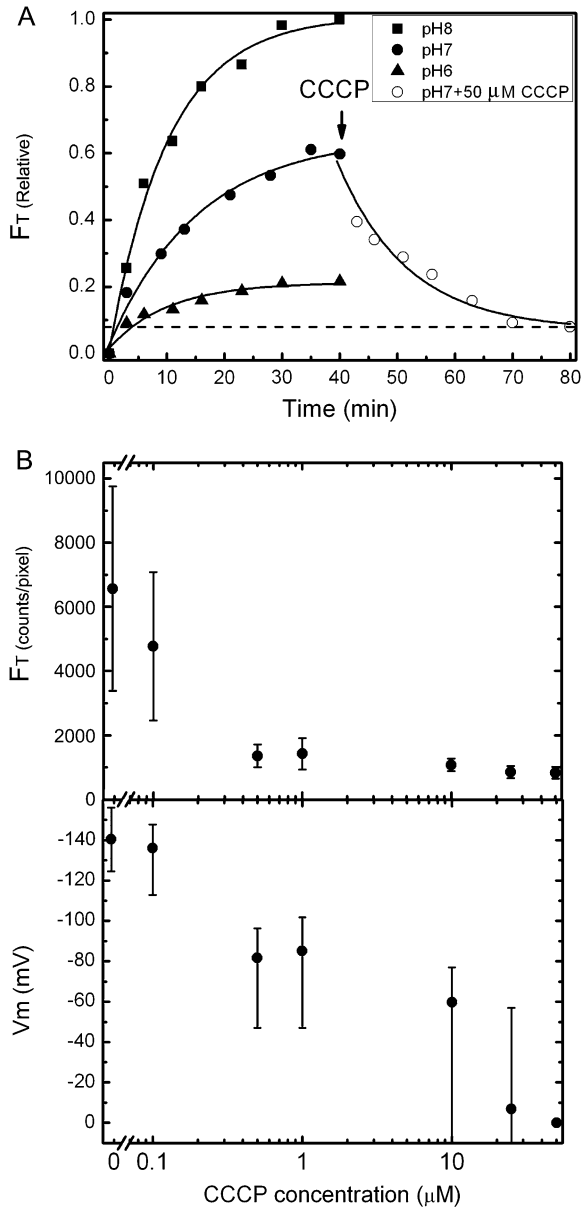

FIGURE 2 (*A*) Total fluorescence intensity (F_T) of cells versus loading time with 0.1 μM TMRM in sodium motility buffer at different pH_{ex} (*solid symbols*), and after treatment with 50 μM CCCP at $pH_{ex} = 7$ (*open circles*). Lines are exponential fits, $F_T = A_0 + A_1 exp\{-t/t_0\}$, time constants t_0 are given in the text. Each point is the mean of measurements of 10 cells. (*B, upper*) F_T versus CCCP concentration. Cells were loaded with TMRM for 40 min and fluorescence measurements were made 40 min after addition of CCCP. Mean $\pm$ SD of 30 cells is shown. (*B, lower*) V_m calculated from the data in the upper panel using the method described in the text.

difference in V_m between cells expressing proton- and sodium-driven motors indicates that V_m is not affected by the extra sodium flux through chimeric motors, as expected if V_m is dominated by the proton cycle in *E. coli* and relatively insensitive to the sodium cycle.

This is further confirmed by the lack of dependence of V_m upon $[Na^+]_{ex}$ (Fig. 3 *B*). The error bars in Fig. 3, *A* and *B*, pH 7 (*squares*), are standard deviations of measurements of

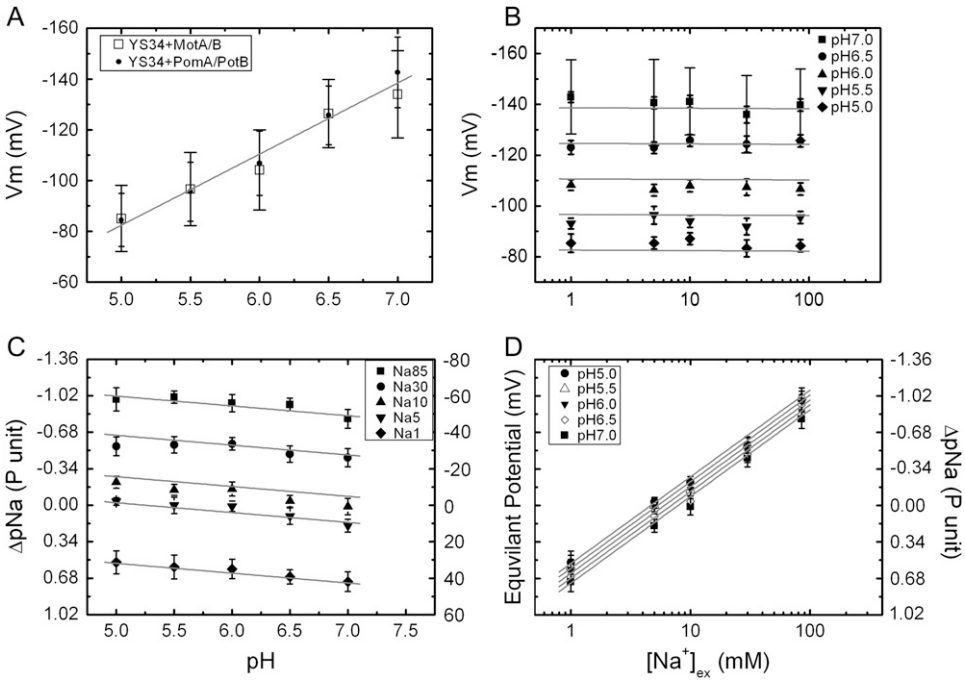

FIGURE 3 (*A*) V_m versus pH_{ex} in cells expressing chimeric PomA/PotB7^E stators (*solid dots*) and in cells expressing wild-type MotA/MotB stators (*open squares*). Mean ± SD of measurements from 50 cells are shown. (*B*) V_m versus $[Na^+]_{ex}$ in different pH_{ex}. Wide-cap error bars indicate standard deviations of measurements of 50 cells, narrow-cap error bars show the standard error of the mean. (*C* and *D*) ΔpNa versus pH_{ex} in different $[Na^+]_{ex}$ (*C*) and versus $[Na^+]_{ex}$ in different pH_{ex} (*D*). Data in *B–D* are from cells expressing chimeric PomA/PotB7^E stators, and error bars in *C* and *D* represent the standard error of the mean. Lines are global fits of all data to the log-linear model described in the text.

50 cells and are considerably larger than the estimated single-cell uncertainty in each measurement of V_m (~3 mV, see Discussion). Thus, the standard deviation reflects intercellular variation in the value of V_m at a given pH_{ex} and $[Na^+]_{ex}$. (Other error bars in Fig. 3 represent the mean ± SE of 50 cells measured.)

We previously reported the dependence of the internal sodium concentration $[Na^+]_{in}$ and the sodium concentration gradient ΔpNa upon $[Na^+]_{ex}$ in *E. coli* at pH 7 (11). Here we use the same method to explore further the dependence of ΔpNa upon pH_{ex} and $[Na^+]_{ex}$ (Fig. 3, *C* and *D*). ΔpNa depends weakly upon pH_{ex} (Fig. 3 *C*) and strongly upon $[Na^+]_{ex}$ (Fig. 3 *D*). We performed least-squares global fits of the dependence of V_m and ΔpNa upon pH_{ex} and $[Na^+]_{ex}$ to a log-linear model:

$$V_m = a + b \times pH_{ex} + c \times \log[Na^+]_{ex}; \quad (10)$$

$$\Delta pNa = d + e \times pH_{ex} + f \times \log[Na^+]_{ex}, \quad (11)$$

where a, b, c, d, e, and f are fitting parameters and $[Na^+]_{ex}$ is in mM. The best-fit parameters for V_m (Fig. 3, *A* and *B*) were $a = 57 \pm 4$ mV, $b = -28 \pm 1$ mV/(pH unit), and $c = 0 \pm 1$ mV/decade. For ΔpNa (Fig. 3, *C* and *D*), the best-fit parameters (expressing ΔpNa in units of mV) were $d = 5 \pm 4$ mV, $e = 5 \pm 1$ mV/(pH unit), and $f = -47 \pm 1$ mV/decade (errors are at 95% confidence limit). The global fits are shown as solid lines in Fig. 3. Thus to a reasonable approximation, V_m depends upon pH_{ex} but not upon $[Na^+]_{ex}$, and ΔpNa depends upon $[Na^+]_{ex}$ but not upon pH_{ex}. This allows independent control of the two components of the SMF using pH and sodium concentration as the control parameters.

Motor speed versus SMF

First we measured the speed of 1-μm polystyrene beads attached to chimeric flagellar motors (11,17) as a function of pH_{ex} and $[Na^+]_{ex}$ (Fig. 4, *A–C*). Fig. 4 *C* shows the data of Fig. 4 *B* as speed versus SMF. The motor speed varies linearly with SMF, from 8.7 to 2.2 Hz/stator over the range −187 to −54 mV. In this high load condition, the two components of SMF, V_m and ΔpNa, are equivalent to within the limits of experimental uncertainty. Similar measurements, using 0.35-μm beads, are shown in Fig. 4, *D–F*. For a given value of $[Na^+]_{ex}$ (and thus also $[Na^+]_{in}$ and ΔpNa), the motor speed varies linearly with SMF as V_m is varied via changes in pH_{ex}. However, the slope, and therefore the motor speed at a given SMF, is lower at low $[Na^+]_{ex}$ than at higher $[Na^+]_{ex}$. V_m and ΔpNa are not equivalent as driving forces of the flagellar motor in the low-load region.

DISCUSSION

Accuracy and error estimation

The sources of error in our single-cell fluorescence V_m measurement are as follows:

1. Random error in measurements of fluorescence intensities F_{in}: the standard deviation of successive measurements of the same cell was typically 3%, attributed to instrumental noise.
2. Focusing error: focusing on the mid-cell plane was judged by the user, introducing a possible source of uncertainty. By repeating the focusing process on the same cell 10 times and reading the *z*-positions from the

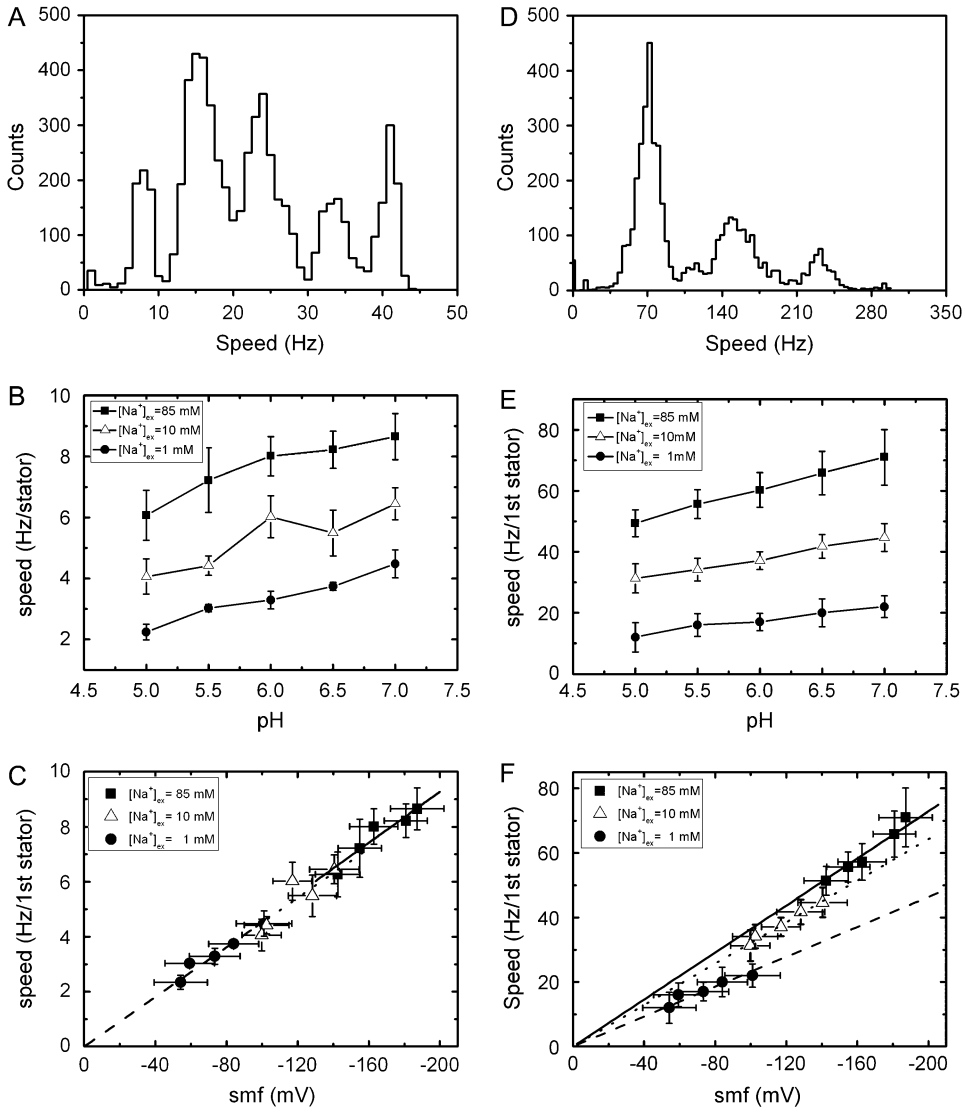

FIGURE 4 The speed of chimeric flagellar motors. (*A*) A histogram of all speeds recorded from 50 different motors driving 1-μm diameter beads at pH 7 and $[Na^+]_{ex}$ = 85 mM. (*B*) Average speed/stator unit with 1-μm beads versus pH_{ex} for different $[Na^+]_{ex}$. (*C*) Speed versus SMF for the data in *B*. (*D*) Histogram of speeds from 25 motors driving 0.35-μm diameter beads at pH 7 and $[Na^+]_{ex}$ = 85 mM. (*E*) Average speed of the first stator unit with 0.35-μm beads, versus pH_{ex} for different $[Na^+]_{ex}$. (*F*) Speed versus SMF for the data in *E*. Also shown in *C* and *F* are linear fits constrained to the origin for data at 1 mM (*dashed lines*), 10 mM (*dotted lines*), and 85 mM (*solid lines*) $[Na^+]_{ex}$. Fitted gradients for 1 mM, 10 mM, and 85 mM $[Na^+]_{ex}$, respectively, are -0.045 ± 0.001 Hz/stator/mV, -0.045 ± 0.002 Hz/stator/mV and -0.046 ± 0.001 Hz/stator/mV in *C*, and -0.23 ± 0.01 Hz/stator/mV, -0.32 ± 0.003 Hz/stator/mV, and -0.36 ± 0.005 Hz/stator/mV in *F*.

piezoelectrical stage driver, we determined a standard deviation of 60 nm in the focusing height. This contributes 2% uncertainty to fluorescence intensity measurements and a further 2% to the value of the correction factor $S(F_{in}/F_{ex})$.

3. Cell-size effect on the correction factor: the diameter of *E. coli* is ~0.8–1.0 μm and the length is ~3 μm. By varying the dimensions of model cells in the optical convolution calculation, we found that variations of cell length had negligible effect on the correction factor, whereas the uncertainty in cell diameter leads to an uncertainty of 11% in the correction factor.
4. Measurement and fitting error in F_{ex}: the fitting error is typically 1%.
5. Membrane binding fluorescence intensity F_m: the fluorescence intensity measurements from cells after CCCP treatment showed a standard deviation of 22%. The relatively high variation may be due to intercellular variation of V_m. The measured standard deviation in V_m of ~15 mV corresponds to a fivefold variation in dye concentration inside the cell; the higher the dye concentration inside the cell, the higher the expected level of membrane binding.

Combining the contributions of these uncertainties to our estimate of V_m (Methods), the uncertainty is <3% at negative values beyond −110 mV, increasing to 5% at −90 mV, 10% at −70 mV, 50% at −40 mV, 100% at −30 mV. Precision at high membrane voltages is helped by the logarithmic nature of the Nernst equation. Under our experimental conditions, V_m in *E. coli* cells had negative values >−80 mV and the uncertainty is <~6%. To increase the accuracy of measurements of low values of V_m, we can calibrate the membrane binding of each individual cell by applying 50 μM CCCP at the end of an experiment, removing this contribution to the uncertainty. By this method, the estimated uncertainty is <5% at −80 mV, 18% at −40 mV, and 100% at −10 mV.

Comparison to other V_m measurements

Our measurements of V_m in single *E. coli* cells are consistent with previous results. Felle et al. measured V_m in *E. coli* using the distribution of radio-labeled permeant cations TPP^+ and $TPMP^+$ (20). The distribution of these ions follows the Nernst equation and their uptake can be determined by dialysis or filtration. They found that V_m increased linearly from -80 mV at pH 5 to -130 mV at pH 7, a slope of -25 mV/pH unit (compared to our measured value of -28 mV/pH unit). Also using *E. coli* and the same experimental method, Castle et al. measured $V_m = -176$ mV at pH 8.5 and -130 mV at pH 6.5 (-23 mV/pH unit) (21), and Minamino et al. (7) measured $V_m = -130$ mV at pH 8.0 and -54 mV at pH 5.0 (-24 mV/pH). Novo et al. measured $V_m = -120$ mV in *Staphylococcus aureus* and *Micrococcus luteus* using the aggregation and redshift of cyanine dye (22). Suzuki et al. measured V_m changes induced by a K^+ diffusion potential in *E. coli* and *Rhodospirillum rubrum* using the aggregation and quenching of carbocyanine dye (23). This cationic dye can permeate the membrane freely and redistributes according to the Nernst equation. The high concentration of dye inside the cell at high V_m causes aggregation and thus quenches the fluorescence of the whole sample. However, the authors did not report measurement of the natural V_m in either species.

Unlike our method, all of the above measurements represent ensemble averages of a large number of cells. Felle et al. measured $V_m = -135$ mV at pH 7 in giant *E. coli* spheroplasts using a patch-clamp micropipette. Although this is a single-cell method, the production of giant spheroplasts is more disruptive than our method and in particular requires disruption of the cell wall, which makes simultaneous measurements of the flagellar motor impossible. Lowe et al. measured $V_m \approx -150$ mV in individual mitochondria in neuroblastoma cells using a method very similar to ours (14). Our data show large intercellular variation, $\sim$15%, in the measured values of V_m at a given pH. We measured similar cell-to-cell variation in ΔpNa at a given $[Na^+]_{ex}$ (11), indicating that individual variation between genetically identical cells extends to both components of the SMF. Based on extrapolation of the linear relationship between motor speed and ΔpNa, we previously predicted that V_m would be -137 mV at pH 7, in close agreement with our measured value of -140 ± 2 mV (mean $\pm$ SE) in this work. We found that $\sim$30 min was required for equilibration of dye concentrations in our experiments, presumably due to relatively low permeability of the outer membrane to dye, after our treatment with EDTA. This limits the time resolution of our technique. Faster response times may be possible by altering our method of permeabilizing the outer membrane, but care would be needed to quantify damage to cells that may be caused by such treatments.

Instability at alkaline pH_{ex}

The pH range 5–7 (Figs. 3 and 4) was chosen because motor rotation was stable over this range. Many chimera motors were unstable at $pH_{ex} = 8$ and sometimes stopped after a brief period of rapid rotation. V_m measurement in cells at $pH_{ex} = 8$ indicated that this was due to a collapse of V_m (see Supplementary Material).

Sodium energetics in *E. coli*

We have shown that V_m in *E. coli* varies linearly with pH_{ex}, and is independent of $[Na^+]_{ex}$ and of the sodium flux through chimeric flagellar motors. This indicates that the membrane voltage is dominated by the balance of proton fluxes, and varies in such a way as to stabilize the PMF and internal pH as pH_{ex} changes (7,21). ΔpNa, on the other hand, depends strongly on $[Na^+]_{ex}$ and only weakly on pH_{ex}, allowing independent control of the two components of the SMF over the ranges -85 to -140 mV in V_m and -60 to $+40$ mV in ΔpNa. Larger values of V_m are possible using alkaline pH, up to a maximum observed in this work of $V_m = -165$ mV and SMF $= -210$ mV, but the SMF is not stable under these extreme conditions in cells expressing Na^+-driven chimeric flagellar motors. There is no strong evidence for the existence of a primary sodium pump in *E. coli*, and the best candidate for maintaining the SMF is the sodium/proton antiporter (24). This is consistent with the weak linkage we observed between the SMF and proton energetics, especially if both components of the PMF are equally effective in maintaining the SMF.

Motor function and SMF or PMF

The relationship between motor speed and ion-motive force has been reported in different bacteria with different methods. Note that swimming speed does not directly reflect motor function in *E. coli* because swimming depends upon the cooperation of flagella in bundles, and therefore early experiments with swimming *E. coli* cells are difficult to interpret. Berg's group showed a linear relationship between motor speed and PMF up to -85 mV in tethered *Streptococcus* cells, using a K^+ diffusion potential and a pH gradient to drive motors on starved cells (5,6). Further studies on glycolyzing tethered *Streptococcus* cells have suggested that the linear relationship between speed and PMF extends up to -150 mV (25). Manson et al. also showed that the pH gradient and V_m were equivalent in tethered *Streptococcus* cells (5). Using a micropipette to energize filamentous *E. coli* cells, with beads acting as markers attached to flagellar motors, Fung and Berg demonstrated the proportionality between speed and V_m up to -150 mV (3). By observing a cell tethered to the coverslip by one motor (operating under high load) and measuring simultaneously the rotation of a second motor on the same cell (operating under lower load, marked by a 0.4-μm-diameter bead), Gabel and Berg showed that the speeds of the two motors were proportional when the PMF was gradually eliminated by adding the ionophore CCCP (4). The high-load motor in this experiment acted as an indicator of the PMF of the cell, as previous work had shown

that speed is proportional to PMF under high load. Thus, the experiment demonstrated that speed varies linearly with PMF under both load conditions, although the relative contributions of V_m and pH gradient were not known. The motor speed of sodium-driven motors in *Vibrio alginolyticus* has a linear dependence upon $\log([Na^+]_{ex})$, but the SMF was not measured (26).

In this work, we manipulated both components of the SMF by changing the pH and sodium concentration of the external medium. Sodium-driven chimeric flagellar motors under high loads imposed by 1-μm beads rotated stably at pH_{ex} between 5 and 7, and speed varied linearly with SMF from -53 to -187 mV, with no detectable difference between the two components of the SMF (Fig. 4 *C*). The two components of SMF were measured separately, with high accuracy, in single cells, and could be controlled on a timescale of ~5 s by rapid exchange of the medium. We did not measure V_m and ΔpNa simultaneously in the same cell due to overlap in the emission spectra of the indicator dyes used for each measurement. Simultaneous measurements would be possible if a different dye were used for one of the measurements. The linear dependence of speed on SMF in the high-load regime is consistent with tight coupling and high efficiency (27): the motor speed is limited neither by internal conformational changes nor by the movement of ions at these speeds. However, in the low-load regime, the motor speed shows different dependence on V_m and ΔpNa (Fig. 4 *F*). Motor speeds in low $[Na^+]_{ex}$ are slower than those in high $[Na^+]_{ex}$ for a given SMF. All previous comparisons of membrane voltage and ion gradient as driving forces for the flagellar motor have been under high load and have found that the two are equivalent, consistent with high efficiency and near-equilibrium behavior. At high speed and low load, we are observing the rates of reactions in the motor cycle far from equilibrium, and under these conditions the ion gradient and membrane voltage are not equivalent. The simplest explanation is that the diffusion-limited binding of sodium ions is the rate-limiting step at low load in low $[Na^+]_{ex}$. By controlling the SMF via V_m and ΔpNa, it is possible to drive the motor purely by V_m, setting ΔpNa at 0. It may also be possible to drive the motor purely by ΔpNa, using CCCP to collapse V_m and transient changes in $[Na^+]_{ex}$ to generate a sodium gradient. Further experiments under various loads are needed for a better understanding of the motor. In particular, it will be interesting to measure torque-speed relationships with different magnitudes and components of the SMF and to use these to test models of the motor mechanism that distinguish between the contributions of electrical and chemical potential.

Driving a 1-μm bead, the motor works in the high-load regime close to thermodynamic equilibrium and the efficiency is close to 100%. For cells in a medium of pH 7 and $[Na^+]_{ex} = 85$ mM, the motor speed is 8.6 ± 0.8 Hz/stator and the SMF is -187 ± 15 mV. The drag coefficient is 20 ± 2 pN nm Hz^{-1} and the work done against viscous drag in one revolution is $1087 \pm 144 \times 10^{-21}$ J/stator. By energy balance, the minimum number of ions needed for one revolution is 36 ± 6, given by the work done divided by the free energy/ion ($-e \times \text{SMF} = 30 \pm 2 \times 10^{-21}$ J). With the motor driving 0.35-μm beads at low SMF ($[Na^+]_{ex} = 1$ mM and pH 5), a minimum of 20 ± 9 ions are required for one revolution, based on a similar calculation. Direct observation of 26 steps/revolution in the chimeric flagellar motor at low load and low SMF (10) indicates that the number of ions required for one step at high load is >1, unless the step size is smaller at high load. At low load, it is likely that the efficiency drops and that the actual number of ions/revolution is greater than the minimum required by energy balance. Sowa et al. (10) observed steps under conditions where motor rotation was unstable. In this work, we have identified conditions for stable slow rotation, which will allow investigation of the statistical properties of motor stepping.

CONCLUSION

Combining single-cell V_m and intracellular sodium measurements, the SMF of cells can be determined. In the pH range 5.0–7.0 and external sodium concentration 1–85 mM, the SMF varies from -53 to -187 mV. The motor speed is stable and varies from 2.2 to 8.7 Hz/stator for 1-μm beads, and from 12.1 to 71.0 Hz for a single stator and 0.35-μm beads. The motor speed when driving 1-μm beads varies linearly with SMF, consistent with tight coupling between ion flux and rotation. The motor speed when driving 0.35-μm beads shows nonequivalent contributions of membrane potential and sodium gradient. Further experiments with different loads are needed to build up a complete motor model. Integration of the fluorescence methods we have described will yield a valuable tool for understanding the energetics and mechanism of the flagellar motor.

SUPPLEMENTARY MATERIAL

An online supplement to this article can be found by visiting BJ Online at http://www.biophysj.org.

We thank Yoshiyuki Sowa for the making of the *E. coli* YS34 chimera strain, Jennifer H. Chandler, and Stuart W. Reid for the *E. coli* YS34 wild-type strain, and David F. Blair for the gift of plasmid (pDFB27).

C.-J.L. thanks the Swire Group/ORS for financial support. The research of R.B. and M.L. was supported by the combined United Kingdom Research Council via an Interdisciplinary Research Collaboration in Bionanotechnolgy, and that of M.L. by a Leverhulme Trust Research Fellowship.

REFERENCES

1. Berry, R. M., and J. P. Armitage. 1999. The bacterial flagella motor. *Adv. Microb. Physiol.* 41:291–337.
2. Berg, H. C. 2003. The rotary motor of bacterial flagella. *Annu. Rev. Biochem.* 72:19–54.

3. Fung, D. C., and H. C. Berg. 1995. Powering the flagellar motor of *Escherichia coli* with an external voltage source. *Nature*. 357: 809–812.

4. Gabel, C. V., and H. C. Berg. 2003. The speed of flagellar rotary motor of *Escherichia coli* varies linearly with protonmotive force. *Proc. Natl. Acad. Sci. USA*. 100:8748–8751.

5. Manson, M. D., P. M. Tedesco, and H. C. Berg. 1980. Energetics of flagellar rotation in bacteria. *J. Mol. Biol.* 138:541–561.

6. Khan, S., M. Meister, and H. C. Berg. 1985. Constraints on flagellar rotation. *J. Mol. Biol.* 184:645–656.

7. Minamino, T., Y. Imae, F. Oosawa, Y. Kobayashi, and K. Oosawa. 2003. Effect of intracellular pH on rotational speed of bacterial flagellar motors. *J. Bacteriol.* 185:1190–1194.

8. Chen, X., and H. C. Berg. 2000. Solvent-isotope and pH effects on flagellar rotation in *Escherichia coli*. *Biophys. J.* 78:2280–2284.

9. Asai, Y., T. Yakushi, I. Kawagishi, and M. Homma. 2003. Ion-coupling determinants of Na^+-driven and H^+-driven flagellar motors. *J. Mol. Biol.* 327:453–463.

10. Sowa, Y., A. D. Rowe, M. C. Leake, T. Yakushi, M. Homma, A. Ishijima, and R. M. Berry. 2005. Direct observation of steps in rotation of the bacterial flagellar motor. *Nature*. 437:916–919.

11. Lo, C.-J., M. C. Leake, and R. M. Berry. 2006. Fluorescence measurement of intracellular sodium concentration in single *Escherichia coli* cells. *Biophys. J.* 90:357–365.

12. Duchen, M. R., A. Leyssens, and M. Crompton. 1998. Transient mitochondrial depolarisations reflects focal sarcoplasmic reticular calcium release in single rat cardiomyocytes. *J. Cell Biol.* 142:975–988.

13. Ehrenberg, B., V. Montana, M.-D. Wei, J. P. Wuskell, and L. M. Loew. 1988. Membrane potential can be determined in individual cells from the nernstian distribution of cationic dyes. *Biophys. J.* 53:785–794.

14. Loew, L. M., R. A. Tuft, W. Carrington, and F. S. Fay. 1993. Imaging in five dimensions: time-dependent membrane potentials in individual mitochondria. *Biophys. J.* 65:2396–2407.

15. Scaduto, R. C., Jr., and L. W. Grotyohann. 1999. Measurement of mitochondrial membrane potential using fluorescent rhodamine derivatives. *Biophys. J.* 76:469–477.

16. Fink, C., F. Morgan, and L. M. Loew. 1998. Intracellular fluorescent probe concentrations by confocal microscopy. *Biophys. J.* 75:1648–1658.

17. Reid, S., M. C. Leake, J. H. Chandler, C.-J. Lo, J. P. Armitage, and R. M. Berry. 2006. The maximum number of torque-generating units in the flagellar motor of *Escherichia coli* is at least 11. *Proc. Natl. Acad. Sci. USA*. 103:8066–8071.

18. Pilizota, T., T. Bilyard, F. Bai, H. Hosokawa, M. Futai, and R. M. Berry. 2007. A programmable optical angle clamp for rotary molecular motors. *Biophys. J.* In press.

19. Leake, M. C., J. H. Chandler, G. H. Wadhams, F. Bai, R. M. Berry, and J. P. Armitage. 2006. Stoichiometry and turnover in single, functioning membrane protein complexes. *Nature*. 443:355–358.

20. Felle, H., J. S. Porter, C. L. Slayman, and H. R. Kaback. 1980. Quantitative measurements of membrane potential in *Escherichia coli*. *Biochemistry*. 19:3585–3590.

21. Castle, A. M., R. M. Macnab, and R. G. Shulman. 1986. Coupling between the sodium and proton gradients in respiring *Escherichia coli* cells measured by ^{23}Na and ^{31}P nuclear magnetic resonance. *J. Biochem. (Tokyo)*. 261:7797–7806.

22. Novo, D., N. G. Perlmutter, R. H. Hunt, and H. M. Shapiro. 1999. Accurate flow cytometric membrane potential measurement in bacteria using diethyloxacarbocynine and a ratiometric technique. *Cytometry*. 35:55–63.

23. Suzuki, H., Z. Wang, M. Yamakoshi, M. Kobayashi, and T. Nozawa. 2003. Probing the transmembrnae potential of bacterial cells by voltage-sensitive dyes. *Anal. Sci.* 19:1239–1242.

24. Padan, E., M. Venturi, Y. Gerchman, and N. Dover. 2001. Na^+/H^+ antiporters. *Biochim. Biophys. Acta*. 1505:144–157.

25. Meister, M., and H. C. Berg. 1987. The stall torque of the bacterial flagellar motor. *Biophys. J.* 52:413–419.

26. Sowa, Y., H. Hotta, M. Homma, and A. Ishijima. 2003. Torque-speed relationship of the Na^+-driven flagellar motor of *Vibrio alginolyticus*. *J. Mol. Biol.* 327:1043–1051.

27. Xing, J., F. Bai, R. M. Berry, and G. Oster. 2006. Torque-speed relationship of the bacterial flagellar motor. *Proc. Natl. Acad. Sci. USA*. 103:1260–1265.